A comprehensive thermal analysis of icemaking process inside a domestic freezer Theoretical, numerical and experimental analyses

Akbar Ahmadi, Ali; Hooman, Kamel; Rahbari, Alireza

DOI
10.1016/j.applthermaleng.2024.122397

Publication date
2024

Document Version
Final published version

Published in
Applied Thermal Engineering

Applied Thermal Engineering 241 (2024) 122397

Contents lists available at ScienceDirect

Applied Thermal Engineering

journal homepage: www.elsevier.com/locate/apthermeng

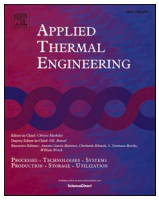

Research Paper

A comprehensive thermal analysis of icemaking process inside a domestic freezer: Theoretical, numerical and experimental analyses

Ali Akbar Ahmadi [a,*], Kamel Hooman [b], Alireza Rahbari [c]

[a] Department of Biomechanics, University of Nebraska at Omaha, Omaha 68182, USA
[b] Process and Energy Department, Delft University of Technology, 2628 CB, the Netherlands
[c] School of Engineering, The Australian National University, ACT 2601, Australia

ARTICLE INFO

Keywords:
Icemaking
Domestic freezer
Volume of fluid method
Enthalpy-porosity method
Solidification

ABSTRACT

Automatic icemakers are integrated into refrigerators to ensure a consistent ice supply and improve energy efficiency. Despite these advantages, a thorough investigation of the automatic icemaking process in domestic refrigerator-freezers is lacking in the literature. This study aims at assessing the performance of automatic icemaking process in a domestic freezer through detailed theoretical, numerical and experimental analyses. A simplistic zero-dimensional transient energy balance model is developed to investigate the heat transfer during different stages of the water solidification process. The convective heat transfer coefficient calculated from the theoretical analysis is used to inform the numerical model. A three-dimensional transient model is proposed to predict the temperature and density variation inside the ice cube modelled as a pyramid. The free surface flow is modelled using volume of fluid method, while enthalpy-porosity method is employed for the water freezing process. The results show a non-uniform temperature distribution throughout the solidification process and that the temperature of the outer frozen layers keeps decreasing with the solidification time. Experiments are conducted to measure the temperature variation of the ice cube. It is shown that the icemaking process is accelerated by around 18 % when the ice-removal temperature is set at −8°C instead of −12 °C, which is a conventional set temperature for ice remover in current domestic freezers.

1. Introduction

In the modern household refrigerators, automatic icemakers are installed in a low-temperature section of the refrigerator to produce ice cubes continuously (see Fig. 1). This cyclic process starts by feeding water into a tray, liquid-phase cooling, water freezing, and deloading the tray [1]. The icemaking process continues till the ice bucket is filled with ice cubes. Driven by the market demand, design and operation of this household appliance has been extensively investigated [2–4]. The refrigerator-freezers account for over 7 % of the average U.S. household energy consumption [5]. Improving the efficiency of domestic refrigerator-freezers significantly affects their electricity consumption [6].

A great deal of effort has been dedicated to evaluate the effect of ambient temperature and the choice of the refrigerant on the energy consumption of domestic refrigerators [7–10]. Ghadiri et al. [10] experimentally investigated the energy consumption and environmental impact of adaptive defrost in domestic refrigerators. Two different domestic refrigerators were tested resulting in 13 % and 5.5 % reduction in energy consumption owing to adaptive defrost function compared with fixed defrost cycles. Moreover, charge level optimization was investigated as a key parameter affecting the overall system cost [11–13]. Rasti and Hwan [14] developed a correlation to predict the refrigerant mass flow rate through an adiabatic and straight capillary tube involving both subcooled and two-phase mixture. In a recent study by Palm [15], the authors revealed that the appropriate selection of condenser and evaporator can potentially decrease the required amount of refrigerant. In the same line of thinking, Hrnjak and Litch [16] assessed the performance of a micro-channel condenser with multi-louvered fins in an ammonia chiller. They reported 53 % reduction in the required mass of refrigerant with a four-times higher overall heat transfer coefficient compared to the classical finned-tube condenser. They investigated the effect of different refrigerants on the cyclic performance of icemaking process [17–19]. As a case in point, Belman-Flores et al. [19] investigated the possibility of using R1234yf instead of R134a to report an optimum charge of R1235yf to be 92.2 g, 7.8 % lower than that of R134a, to deliver 130 W of cooling load under the

* Corresponding author.
E-mail address: aahmadi@unomaha.edu (A. Akbar Ahmadi).

https://doi.org/10.1016/j.applthermaleng.2024.122397
Received 9 September 2023; Received in revised form 13 December 2023; Accepted 6 January 2024
Available online 14 January 2024

Nomenclature

A	Area, m^2
A_{mush}	Mushy zone constant
B	Length of water, m
C	Width of water, m
Ca	Capillary number
c_p	Specific heat at constant pressure, J/kg.K
c_v	Specific heat at constant volume, J/kg.K
D	Length of air, m
E	Width of air, m
F	Height of water, m
F_σ	Volumetric surface tension, N/m^3
G	Height of air, m
g	Gravity acceleration, m/s^2
h	Convective heat transfer coefficient, $W/m^2.K$
H	Enthalpy, J/kg
k	Thermal Conductivity, W/m.K
L	Charactristic length, m
L_f	Latent heat of fusion, KJ/kg
m	Mass, kg
n	Unit normal vector, m
Nu	Nusselt number
p	Pressure, Pa
$\dot{Q}$	Heat rate, W
Ra	Rayleigh Number
S	Momentom source term, N/m^3
t	Time, s
T	Temperature, °C
u	Velocity vector, m/s
U	Velocity, m/s
$\dot{U}$	Internal energy, W

Greek symbols

α	thermal diffusivity. m^2/s
α_j	Volume of fraction of the jth phase
α_{liquid}	Liquid volume fraction
β	Expansion coefficient, 1/K
θ	Angle of ice cube front surface, °
θ_d	Dynamic contact angle, °
θ_{eq}	Equilibrium contact angle, °
κ	Curvature
μ	Dynamic Viscosity, Pa.s
ρ	Density, kg/m^3
σ	Surface tension, N/m
τ_s	Unit tangential vector, m
φ	Angle of ice cube side surface, °

Subscripts

0	Initial
CL	Contact line
F	Freezing
liquid	liquidus
ref	reference
solid	solidus
w	water

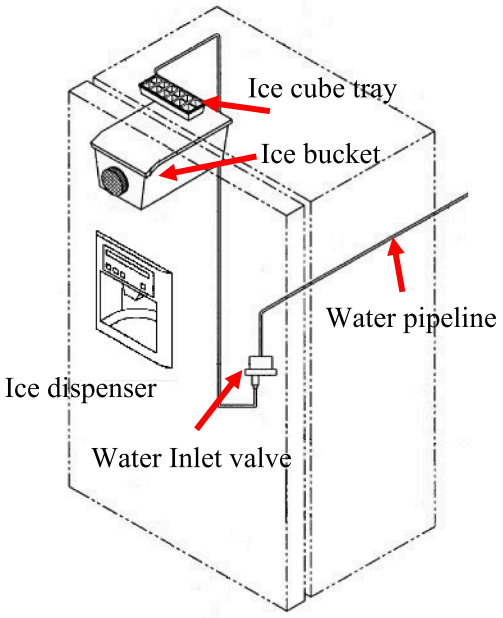

Fig. 1. Schematic view of an upright freezer including an automatic icemaker circuit including ice cube tray, ice bucket, ice dispenser, water inlet valve, and water pipeline.

same working conditions.

Icemaking imposes an additional refrigeration load to a refrigerator as it involves freezing water. Within the context of ice production in household freezers, two primary areas of interest emerge: one involves refining models to enhance the accuracy of electricity consumption measurements, while the other centers around devising a robust numerical approach to comprehensively simulate the icemaking process. Considering the initial objective, Meier and Martinez [20] and Haider et al. [21] were among the first who established the procedure of measuring the electricity consumption of icemaking process in domestic refrigerator. To further improve the model suggested by above, Yashar and Park [22] came up with a more comprehensive method to measure the energy consumption considering four refrigerator-freezers configurations. Regarding the second objective, Michałek and Kowalewski [23] used the enthalpy-porosity fixed-grid and volume of fluid (VOF) methods to simulate the phase change and free surface flow and obtain tow-dimensional transient solutions for the water freezing process. Bourdillon et al. [24] developed a numerical model based on the enthalpy-porosity method to study the icemaking process in OpenFOAM. The model is linked with a slurry-mushy formulation, where the partially solidified region is divided into two distinct zones based on the ice volume fraction. Several authors have employed different numerical approaches to simulate this phenomenon using finite volumes and Lagrangian methods [25–28].

There is a consensus that incorporating an automatic icemaker aligns with the current industry practice for two reasons: (i) ensuring a constant supply of ice and (ii) minimzing the need to repeatedly open the freezer door, resulting in a more energy-efficient refrigerator. Despite these benefits, there is a gap in literature regarding an in-depth study on the automatic icemaking process in domestic refrigerator-freezers. This requires a thorough modeling and experimental assessment of the solidification process within ice trays. The challenge lies in measuring the temperature at the center of the ice, crucial for determining the proper timing for ice cube removal and preventing premature extraction. In view of the above, an experimental setup is designed to measure the temperature and solidification time of the ice cube. This is coupled with a three-dimensional transient modelling of ice cube modelled as a pyramid trunk using enthalpy-porosity and volume of fluid models. The convective heat transfer coefficient around the ice cube is calculated

based on theoretical correlations.

2. Definition of the automatic icemaking

Automatic icemaking consists of three main stages including water filling, icemaking, and ice removal. A representation of the icemaker installed on a commercial product is shown in Fig. 2. During the water filling stage, water is supplied to the ice tray through the pipeline in a predetermined time, usually taking four to five seconds. Afterward, water freezes and is automatically ejected from the ice tray at a specific temperature which is monitored by a temperature sensor installed under the ice tray. The icemaker assembly comprises a driving tool that produces a rotary force for the ice tray. To transfer ice cubes to an underlying ice bucket, the ice tray is rotated by the arm. An ice checkup sensor lever is connected to the driving tool to detect the ice mass in the ice bucket. The ice tray is then flipped while the ice checkup sensor lever moves down into the ice bucket to ensure it is emptied.

Fig. 3 shows this process by demonstrating the evolution of the water temperature. Three stages are defined: (i) water at ambient temperature flows into the ice tray, which is then cooled to 0 °C with sensible heat transferred to cooling air, (ii) water freezing through further removal of latent heat from water, and (iii) the heat transferred from the ice cubes decreases the ice temperature to a certain design point.

3. Experimental analysis

3.1. Experimental procedure

Specifications of the domestic freezer studied here are summarized in Table 1. The test begins when the water inlet valve opens and 97 mm^3 of water flows to the ice tray through the designated pipeline. Temperature of the ice tray is measured by the negative temperature coefficient (NTC) thermistor installed under the ice tray and once −12 °C is reached, the driving tool rotates the ice tray and the ice cubes fall into the ice bucket.

The experimental procedure consists of temperature measurement of freezer compartments and the icemaker. The freezer temperature is taken as the arithmetic average of seven local temperature values measured in different locations inside the freezer compartment as shown in Fig. 4. temperature sensors are positioned and installed according to ISO 15502. In addition, temperatures of icemaker and that of the ambient air are monitored and recorded continuously using T-type thermocouples.

Temperature and pressure of inlet water, the total mass of ice made during a day as well as the time it takes to make ice are measured. These measurements are carried out at the ambient condition of 32 ± 0.5 °C and the ambient relative humidity of 50 ± 3 % as per the recommendations of ISO 15502. Water enters the freezer at the ambient temperature of 32 ± 0.5 °C and ice is removed when the ice tray temperature reaches −12 ± 0.5 °C. The experiments were repeated five times over a range of freezer cabin temperature of −16 °C to −24 °C.

3.2. Experimental setup

Experiments are conducted in a walk-in type chamber (see Fig. 5) to ensure that controlled and constant ambient conditions (the surrounding temperature and relative humidity) are set during the experiments. The freezer is positioned inside the climate chamber. Water flows into the ice tray from a reservoir, located inside the chamber, with a constant temperature of 32 ± 0.5 °C and pressure of 5 ± 0.05 bar. A pressure sensor (P1600-200, pace Scientific Inc., USA) with accuracy of 1 % is used to monitor the inlet water pressure. In this study, 97 ± 0.5 mm^3 of water, measured by a graduated cylinder, fills the ice tray within 4.5 s controlled using a built-in PCB.

Voltage and current, active power and reactive power, as well as power factor are recorded continuously using a data acquisition system. Energy consumption of the freezer is calculated by analyzing the data and the ON time ratio. The ON time ratio is obtained by dividing the operating time of the compressor by the total cycle time. Initially the freezer is turned on and set to a desired temperature. The icemaker is switched on when these conditions are satisfied. The accuracy of our measurements is listed in Table 2. The uncertainty of water flow rate and water temperature is within ± 0.5 % according to [29] and ± 2.1 %, respectively. Furthermore, each test was repeated five times with relative standard deviation of flow and temperature measurements obtained as 2.9 % and 2.2 %, respectively.

4. Numerical analysis

4.1. Problem statement

Fig. 6 depicts the computational domain wherein blue shade denotes water phase and air phase is shown in white. To reduce computational time, only a quarter of the ice cube is modeled based on the symmetry assumption made here. Dimensions of the computational domain are listed in Table 3. Air pressure is prescribed using pressure outlet boundary condition. The temperatures within the computational domain are initially set to the freezer temperature for air (-24 °C) and 32 °C for water.

4.2. Governing equations

The numerical solution of the governing equations is achieved through a combination of enthalpy-porosity and VOF methods. The physical domain is discretized into solid, liquid, and mushy regions. The

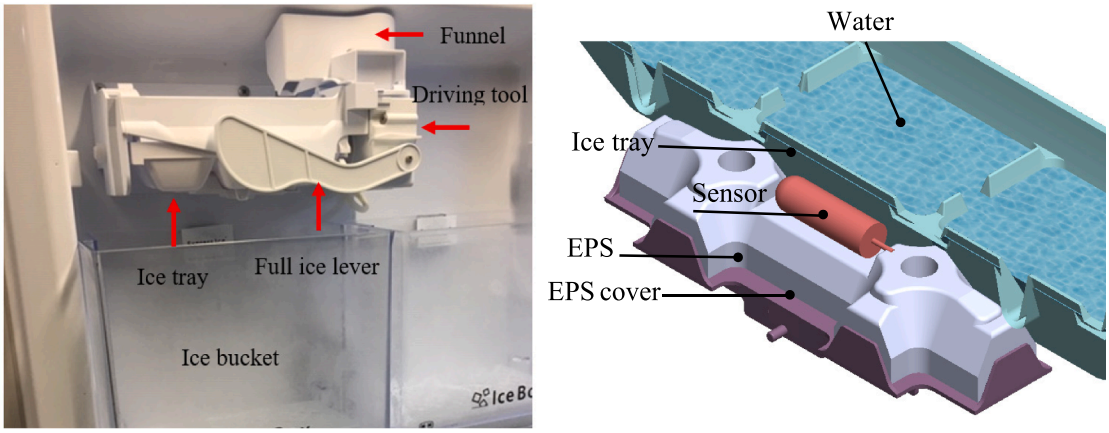

Fig. 2. Automatic icemaker installed on a freezer and the location of temperature sensor.

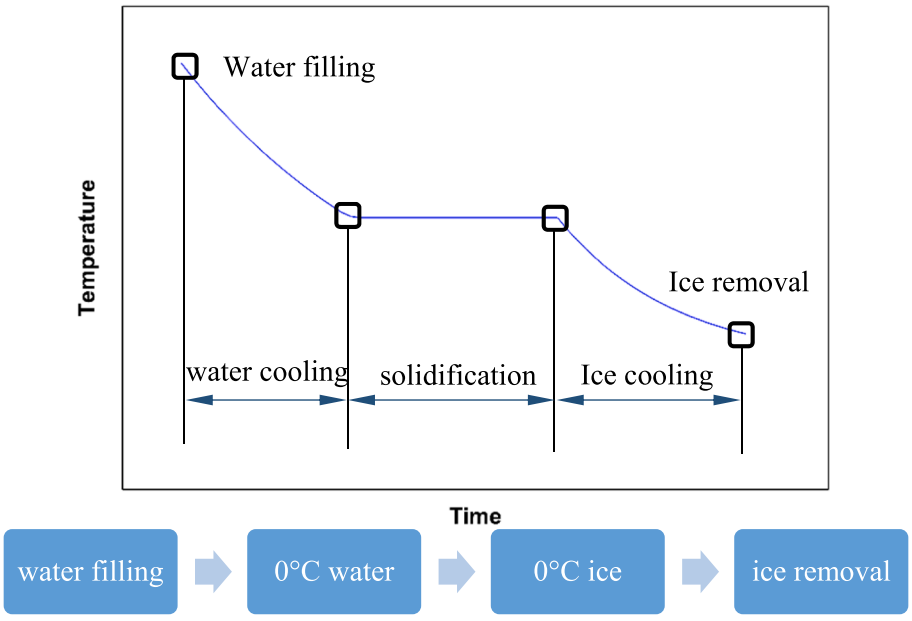

Fig. 3. Ice cube temperature as a function of time indicating various stages in the icemaking process.

Table 1
Technical specifications of the studied freezer.

Capacity	350 L
Freezer cabin net volume	290 L
Voltage	220–240 Volt
Rated current	0.5 Amper
Frequency	50 Hz
Refrigerant	R600a, 65 gr
Defrost	Auto defrost
Capillary tube length	320 cm
Climate class	Tropical

tracking of the interface between the phases is accomplished by solving a continuity equation for the volume fraction of one or more of the phases [30]:

$$\frac{\partial}{\partial t}(\alpha_j \rho_j) + \nabla.(\alpha_j \rho_j \boldsymbol{u}) = 0 \tag{1}$$

where ρ and u are the density and velocity vector respectively. In this equation, α_j is the volume of jth phase over the cell volume.

$$\alpha_1 = \begin{cases} 0 & \text{if the cell is occupied by liquid} \\ 0 < \alpha_j < 1 & \text{if the cell contains liquid and gas} \\ 1 & \text{if the cell is occupied by gas} \end{cases} \tag{2}$$

in which:

$$\alpha_1 + \alpha_2 = 1 \tag{3}$$

The momentum conservation equation is written as:

$$\frac{\partial(\rho \boldsymbol{u})}{\partial t} + \nabla\cdot(\rho \boldsymbol{u}\boldsymbol{u}) = -\nabla p + \nabla\cdot\mu\left[\left(\nabla \boldsymbol{u} + \nabla \boldsymbol{u}^{\mathrm{T}}\right)\right] + \rho \boldsymbol{g} + S + F_\sigma \tag{4}$$

where p, μ, g, S, and F_σ represent the pressure, dynamic viscosity, gravitational acceleration, momentum source term, and volumetric surface tension force, respectively. The momentum source term due to decreased porosity in the mushy zone is expressed as:

$$S = \frac{\left(1 - \alpha_{\text{liquid}}\right)^2}{\left(\alpha_{\text{liquid}}{}^3 + \varepsilon\right)} A_{\text{mush}} \boldsymbol{u} \tag{5}$$

Fig. 4. The location of thermocouples installed inside the freezer.

where α_{liquid}, ε, and A_{mush} are the liquid volume fraction, small number to prevent division by zero, and mushy zone constant respectively.

The volumetric surface tension force is a function of surface tension, σ, gradient of volume fraction, α_1, local curvature of the free surface, κ, and the average density:

$$F_\sigma = \sigma \frac{\rho \kappa \nabla \alpha_1}{\frac{1}{2}(\rho_1 + \rho_2)} A_{\text{mush}} \boldsymbol{u} \tag{6}$$

Fig. 5. Walk-in type test room to ensure controlled and constant ambient conditions during experiments.

Table 2
The accuracy of the test room and measurement tools.

Ambient temperature	± 0.5 °C
Relative humidity	3.0 %
Thermocouple (T-type)	± 0.25 °C
Voltage stabilizer	± 0.1 V
Power sensor	0.05 %
Current sensor	0.05 %
Pressure sensor	1.0 %
Graduated Cylinder	± 0.5 mm^3
anemometer	± 0.2 m/s

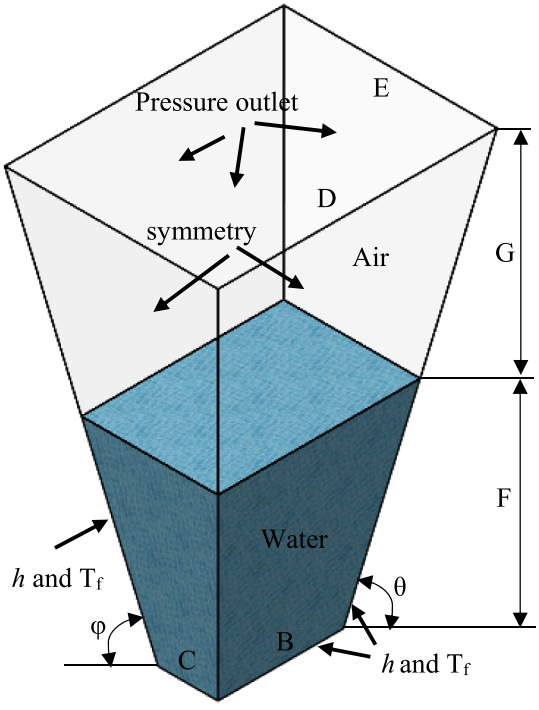

Fig. 6. A quarter of an ice cube analyzed in the numerical simulation.

Table 3
Dimensions description of the under-study ice cube.

B (mm)	C (mm)	D (mm)	E (mm)	F (mm)	G (mm)	θ (degree)	φ (degree)
14	6.7	31.3	23.9	20	20	66.7	66.8

where

$$\kappa = \nabla\cdot\boldsymbol{n}, \boldsymbol{n} = \frac{\nabla\alpha_1}{|\nabla\alpha_1|} \tag{7}$$

where $\boldsymbol{n}$ is the normal vector of gas–liquid interface. At the contact line (CL), the adhesion force is calculated from the contact angle, θ_d, by:

$$\boldsymbol{n}_{CL} = \left(\frac{\nabla\alpha_1}{|\nabla\alpha_1|}\right)_{CL} = \boldsymbol{n}_s\cos\theta_d + \boldsymbol{\tau}_s\sin\theta_d \tag{8}$$

where $\boldsymbol{n}_s$ and $\boldsymbol{\tau}_s$ are the unit vectors normal and tangential to the solid surface, respectively. In this equation, the contact angle is obtained from:

$$\theta_d = f_{Hoff}\left[Ca + f_{Hoff}^{-1}(\theta_{eq})\right] \tag{9}$$

in which $f_{Hoff}(x)$ in the Hoffman function given by:

$$f_{Hoff} = \arccos\left\{1 - 2\tanh\left[5.16\left(\frac{x}{1+1.31x^{0.99}}\right)^{0.706}\right]\right\} \tag{10}$$

where $f_{Hoff}^{-1}(x)$ is the inverse function of $f_{Hoff}(x)$. Further, $Ca = \mu U_{CL}/\sigma$ is the Capillary number and θ_{eq} is the equilibrium contact angle. The details of the VOF and contact angle models can be found in the published literature [31].

The energy equation is represented as:

$$\frac{\partial(\rho H)}{\partial t} + \nabla\cdot(\rho\boldsymbol{u}H) = \nabla\cdot(k\nabla T) \tag{11}$$

where H, k, and T represent the total enthalpy, thermal conductivity, and temperature, respectively. The total enthalpy in each cell is calculated as the sum of sensible enthalpy, h, and latent heat, ΔH:

$$H = h + \Delta H = h_{ref} + \int_{T_{ref}}^{T} c_p dT + \alpha_{liquid}L_f \tag{12}$$

where h_{ref}, c_p, and L_f are the reference enthalpy at the reference temperature T_{ref}, specific heat, and latent heat, respectively. The liquid volume fraction is calculated from the following equation:

$$\alpha_{liquid} = \begin{cases} 0 & \text{if} T < T_{solid} \\ \dfrac{T - T_{solid}}{T_{liquid} - T_{solid}} & \text{if} T_{solid} < T < T_{liquid} \\ 1 & \text{if} T > T_{liquid} \end{cases} \tag{13}$$

where T_{solid} and T_{liquid} are the solidus and liquidus temperature set at 273 K and 273.3 K, respectively [23].

The thermophysical properties of the water, ice, and air are defined in Table 4. Air is modelled as dry air with ideal gas model. For the range

Table 4
Material properties of the air, water, and ice used in the numerical model [32,33].

properties	Material		
	Ice	Water	Air
Density (kg/m^3)	918	999	1.39
Specific heat capacity (J/kgK)	2024	4198	1005.4
Thermal conductivity (W/mK)	1.99	0.591	0.0226
Viscosity (kg/ms)	–	Eqs. (15)	16.25×10^{-6}
Expansion coefficient (1/K)	15.4×10^{-5}	Eqs. (14)	0.00367
Latent heat of diffusion (kJ/kg)	333.9	333.9	–

of water temperature considered in this research, the thermophysical properties do not change significantly with the temperature except for its thermal expansion coefficient and viscosity which are modelled as [32]:

$$\beta_w = -0.0861 + 0.0008\mathrm{T} - 3\times10^{-6}T^2 + 3\times10^{-9}T^3 \quad (14)$$

$$\mu_w = 0.3693 - 0.0036T + 1\times10^{-5}T^2 - 1\times10^{-8}T^3 \quad (15)$$

where temperature is in K.

4.3. Numerical solution

Structured quadratic mesh is adopted for this study with a finer mesh at the interface to capture sharp gradients. Fig. 7 shows the generated mesh of the ice cube. Grid independence is conducted by running the simulations on 40000, 96,300 and 288,000 cells. As seen in Fig. 8a, increasing the number of mesh elements beyond 96,360 has a negligible effect on the solidification time. As such, the optimum cell number was found to be 96360. A sensitivity analysis was conducted to evaluate the effect of time step on the accuracy of the results. As seen in Fig. 8b, there is a slight variation in the solidification time with the time step sizes smaller than 1 ms. Hence, the time step of 1 ms is chosen in this study.

5. Theoretical model

A theoretical model is developed to analyze the heat transfer from the icemaker to allow predicting the total time required for icemaking. The time for a specific amount of water to freeze from the inlet temperature T_{w_0} to the desired temperature T_{w_d} is formulated by considering the ice tray as the control volume (see Fig. 9).

The energy balance is expressed as:

$$\dot{Q}_{\mathrm{tot}} = \Delta\dot{U} \quad (16)$$

Where $\dot{Q}_{tot}$ indicates the amount of heat transferred to the control volume and $\Delta\dot{U}$ denotes a change in the internal energy of the control mass. The water inside the ice tray is cooled through convection heat transfer to the cold air in the freezer. Conduction heat transfer through the thin highly-conducting ice tray shell is neglected. Transient heat transfer from water to its surrounding is expressed as:

$$-hA\left(T_{\mathrm{w}} - T_{\mathrm{f}}\right) = mc_v\frac{\mathrm{d}T_{\mathrm{w}}}{\mathrm{d}t} \quad (17)$$

where T_{w}, T_{f}, m, c_v, A, and h represent the water and freezer air temperature, the mass of water inside the ice tray, the specific heat capacity of water, the total surface of the water inside the ice tray (equal to 28572 mm^2 for the test set up described above), and the convective heat transfer coefficient. Eq. (17) can be solved to prescribe the water temperature as a function of time. To this end, there are three stages occurring as illustrated in Fig. 3.

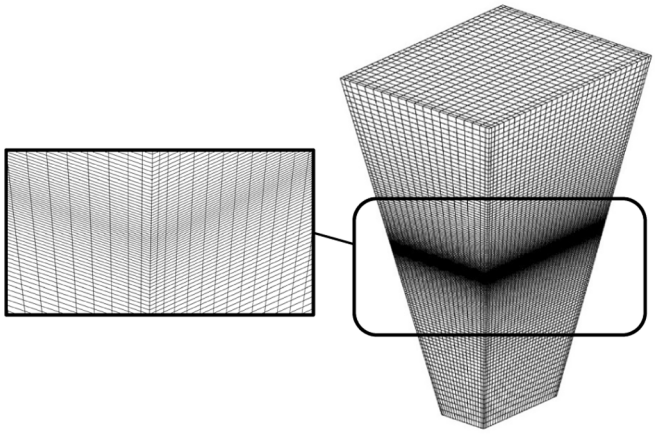

Fig. 7. Close-up of the generated mesh of the ice cube.

Stage 1: Energy transferred from the control mass leads to a decrease in the liquid water temperature (until 0 °C is reached).

$$T_{\mathrm{w}} = \mathrm{e}^{\frac{-t(hA)}{mC_v}}\left(T_{\mathrm{w}_0} - T_{\mathrm{f}}\right) + T_{\mathrm{f}} \quad (18)$$

where T_{w} is the water temperature at a given time t.

Stage 2: The temperature cannot decrease until water fully freezes. Hence, the energy transferred from the water leads to the formation of ice.

$$hA\left(273.15 - T_{\mathrm{f}}\right) = \frac{mL_{\mathrm{f}}}{t} \quad (19)$$

where L_{f} represents the latent heat of fusion.

Stage 3: Once the solidification process is complete, the energy balance is similar to that of stage 1 and lumped formulation leads to:

$$-hA\left(T_{\mathrm{ice}} - T_{\mathrm{f}}\right) = mc_v\frac{\mathrm{d}T_{\mathrm{ice}}}{\mathrm{d}t} \quad (20)$$

$$T_{\mathrm{ice}} = \mathrm{e}^{\frac{-thA}{mc_v}}\left(T_{\mathrm{ice}_0} - T_{\mathrm{f}}\right) + T_{\mathrm{f}} \quad (21)$$

where T_{ice} is the ice temperature and thermophysical properties are those of ice (during stage 3) while those of liquid water were used during stage 1.

The heat transfer coefficient h for horizontal and inclined plates are expressed in terms of the Nusselt number:

$$Nu = 0.54\mathrm{Ra}_L{}^{0.25} \quad (22)$$

where Ra is the Rayleigh number defined as [33]:

$$\mathrm{Ra}_L = \frac{\cos\theta g\beta\left(T_{iw} - T_{\mathrm{f}}\right)L^3}{\alpha\vartheta} \quad (23)$$

where $\cos\theta$ is the inclination angle. Properties of air around the icemaker are evaluated at the film temperature.

6. Results and discussion

6.1. Theoretical result

The average Nusselt number and the convective heat transfer coefficient for three different freezer temperatures are presented in Table 5. The convective heat transfer coefficient values are used in the numerical simulations. Table 6 presents the freezing process time in each stage when water flows to the ice tray (initially at 32 °C). Fig. 10 shows the ice tray temperature as a function of time. As seen, around 72 % of icemaking time is spent on stage 2 (green line) when the heat transferred from the liquid water matches with the latent heat of fusion. Moreover, a sharp decrease in the ice tray temperature during stages 1 and 3 is observed. Different rates are attributed to different thermophysical properties of ice and liquid water during stages 1 and 3.

Fig. 11 shows the convective heat transfer coefficient and average Nusselt number as a function of freezer temperature. Lower freezing chamber temperature slightly increases the heat transfer coefficient through higher Ra values. By decreasing the freezer temperature from −16 to −24 the total Nu and h enhances by almost 10 % and 9 %, respectively. Note that the Nu values are lower on the side surfaces (for their smaller length scale). Moreover, the gravitational force acting on the fluid is reduced by a cosθ factor compared with the horizontal surfaces hence the fluid velocities along these plates are reduced leading to lower convection heat transfer. The area-weighted average for heat transfer coefficient is then obtained and used in the analysis.

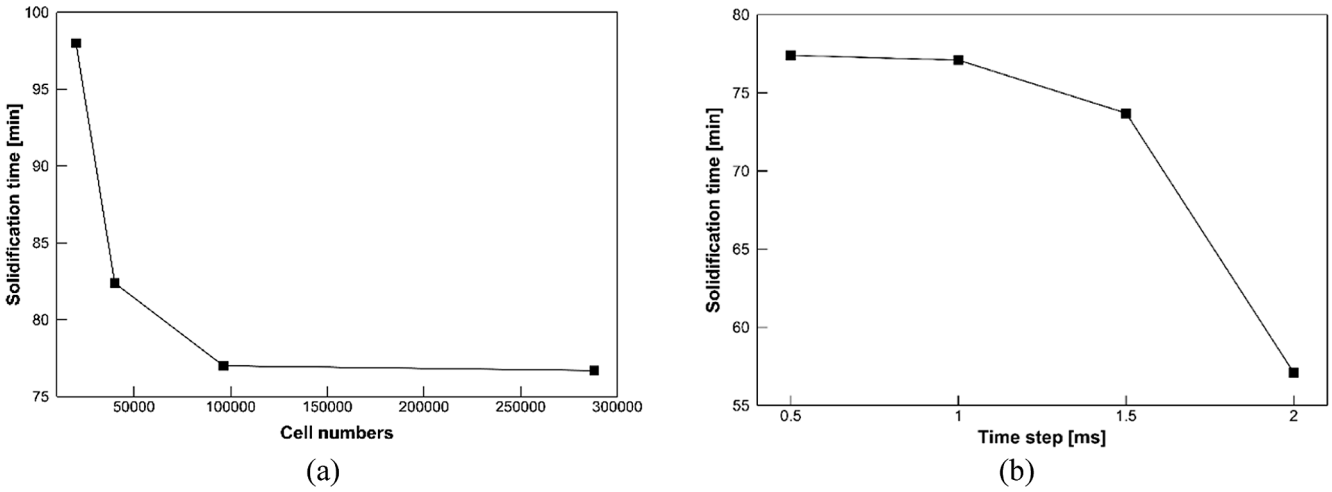

Fig. 8. Variation of solidification time as a function of: (a) cell numbers and (b) time step.

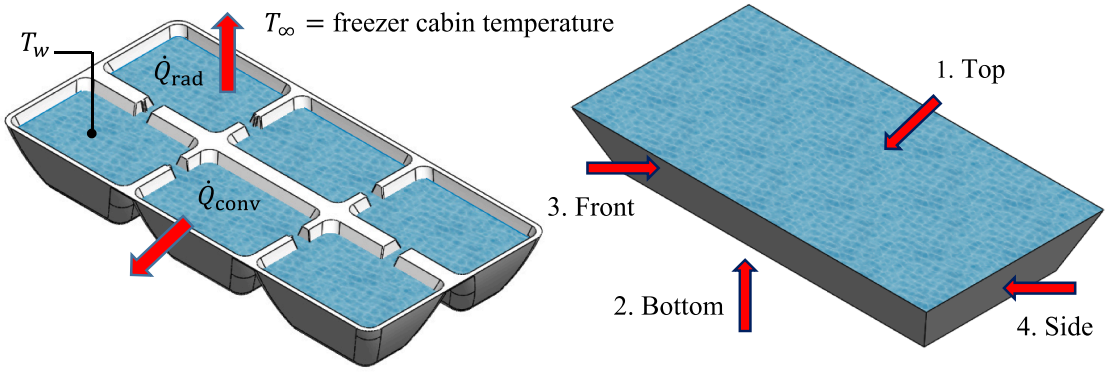

Fig. 9. Schematic view of the ice tray analyzed in this research.

Table 5
Nusselt number and free convection coefficient at different freezer cabin temperatures.

Surface	Freezer at −24 °C		Freezer at −20 °C		Freezer at −16 °C	
	h (W/m^{2}K)	Nu	h (W/m^{2}K)	Nu	h (W/m^{2}K)	Nu
Top	8.21	7.96	7.86	7.56	7.40	7.10
Bottom	4.89	4.08	4.75	3.92	4.54	3.73
Side	6.60	2.48	6.40	2.38	6.12	2.26
Front	6.31	2.75	6.05	2.64	5.77	2.51

Table 6
Freezing process time for each stage when the freezer temperature is −24, −20 and −16 °C.

Stage	Time in each stage (minutes)		
	−16 °C	−20 °C	−24 °C
Stage 1	27.4	23.2	21.5
Stage 2	118.7	92.9	76.2
Stage 3	17.5	11.1	8.5
Total time	163.6	127.2	106.2

6.2. Experimental result

Fig. 12 presents a comparison between experimental and analytical data. Icemaking time was measured experimentally with the freezer temperature ranging from −16 °C to −24 °C with 2 °C interval at ambient temperature of 32 °C. As seen in this figure, there is a reasonable agreement between the results obtained from the theoretical model and experimental data with the maximum error being under 3 %.

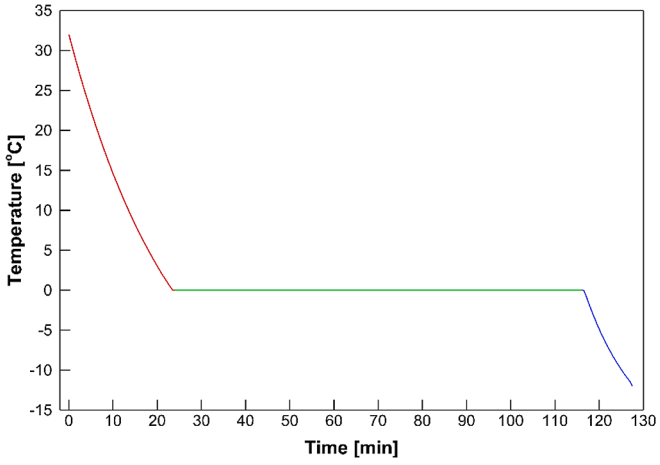

Fig. 10. Icemaking process from water filling to ice removal obtained from the theoretical solution considering ambient temperature of 32 °C and freezer temperature of −20 °C.

Fig. 13 shows the ice tray temperature obtained from the experiment as a function of time. The ice tray temperature rapidly drops during stage 1, then remains constant during stage 2 for a long time and finally

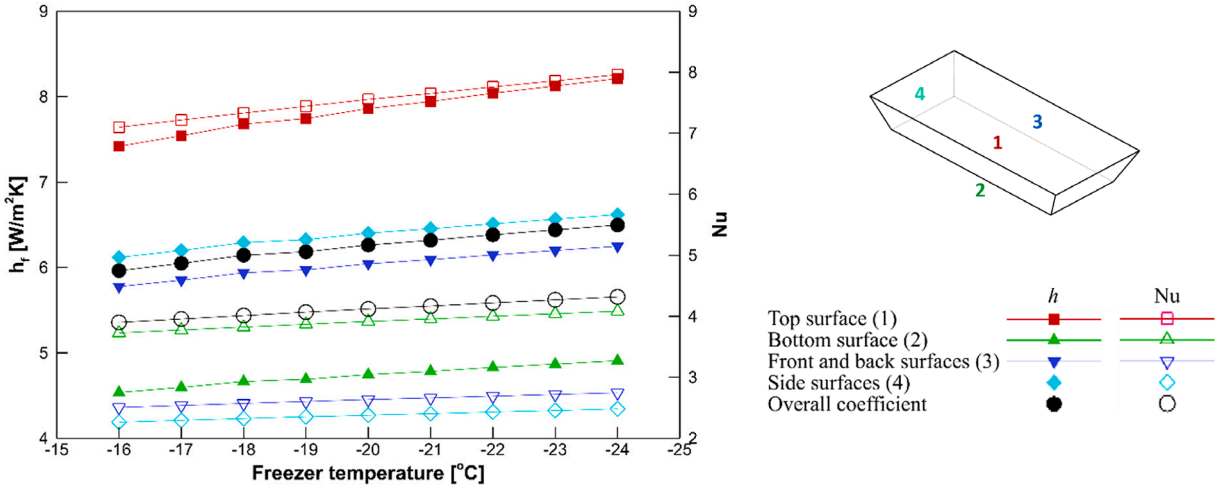

Fig. 11. Free convection heat transfer coefficient and Nusselt number for top, bottom, front, and side surfaces.

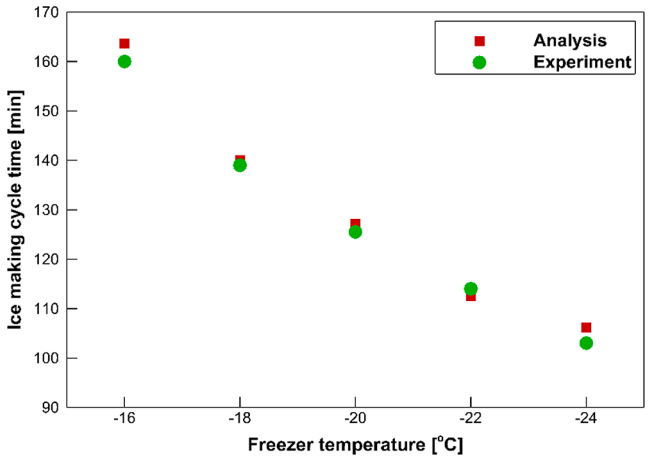

Fig. 12. Comparison of icemaking time as a function of freezer cabin temperatures obtained from the analytical and experimental data.

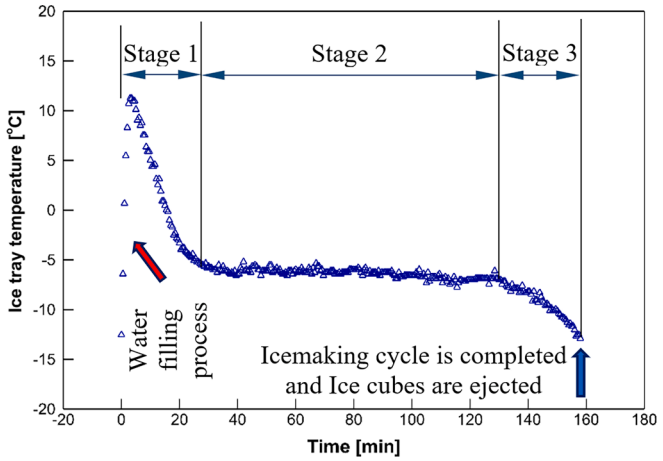

Fig. 13. Icemaking process from water filling to ice removal obtained from the experiment considering freezer temperature of −16 °C.

reduces with a fast rate approaching that of the freezer air during stage 3. The ice tray temperature, right before water being supplied, is close to that of the freezer air. With the flow of water at a higher temperature of 32 °C, the ice tray temperature quickly responds to the heat transferred from water. During water filling process, which takes around 5 s, the ice tray temperature increases from −12 °C to about 13 °C. It is also interesting to note that the ice tray temperature is lower than 0 °C during stage two. The icemaker sensor is located under the ice tray and is covered and isolated by an EPS (see Fig. 2). Even with this isolation, freezer temperature affects the icemaker sensor. As seen in this figure, the EPS is in direct contact with the ambient air inside the freezer. As a result, the reading of the sensor is not only influenced by the temperature of the water but also by the chilled air surrounding the ice tray. This causes the sensor to display a lower phase change temperature from the experiment compared to the theoretical (see Fig. 10) and numerical (see Fig. 16) results.

Fig. 14 illustrates the evolution of the ice tray temperature with time at three freezer temperatures of −16 °C, −20 °C, and −24 °C. As seen, the process stops when ice tray temperature reaches −12 °C. While the overall trends are similar, lower freezer temperature shortens the solidification time. The freezing time is improved by 30 % and 60 % when the freezer temperature is −24 °C compared to −20 °C and −16 °C, respectively.

6.3. Numerical result

The results of numerical simulation for the freezing process are shown in Fig. 15. At the start of the simulation (t = 0), the freezer temperature is −24 °C while the water temperature is set at 32 °C. As

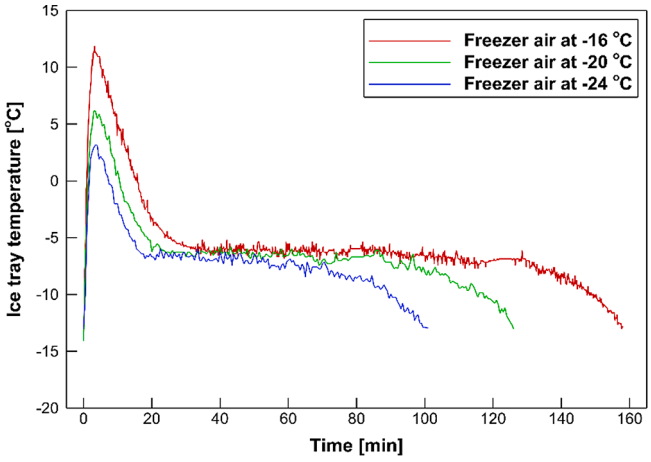

Fig. 14. Icemaking process from water filling to ice removal obtained from the experiment considering freezer temperature of −16 °C, −20 °C, and −24 °C.

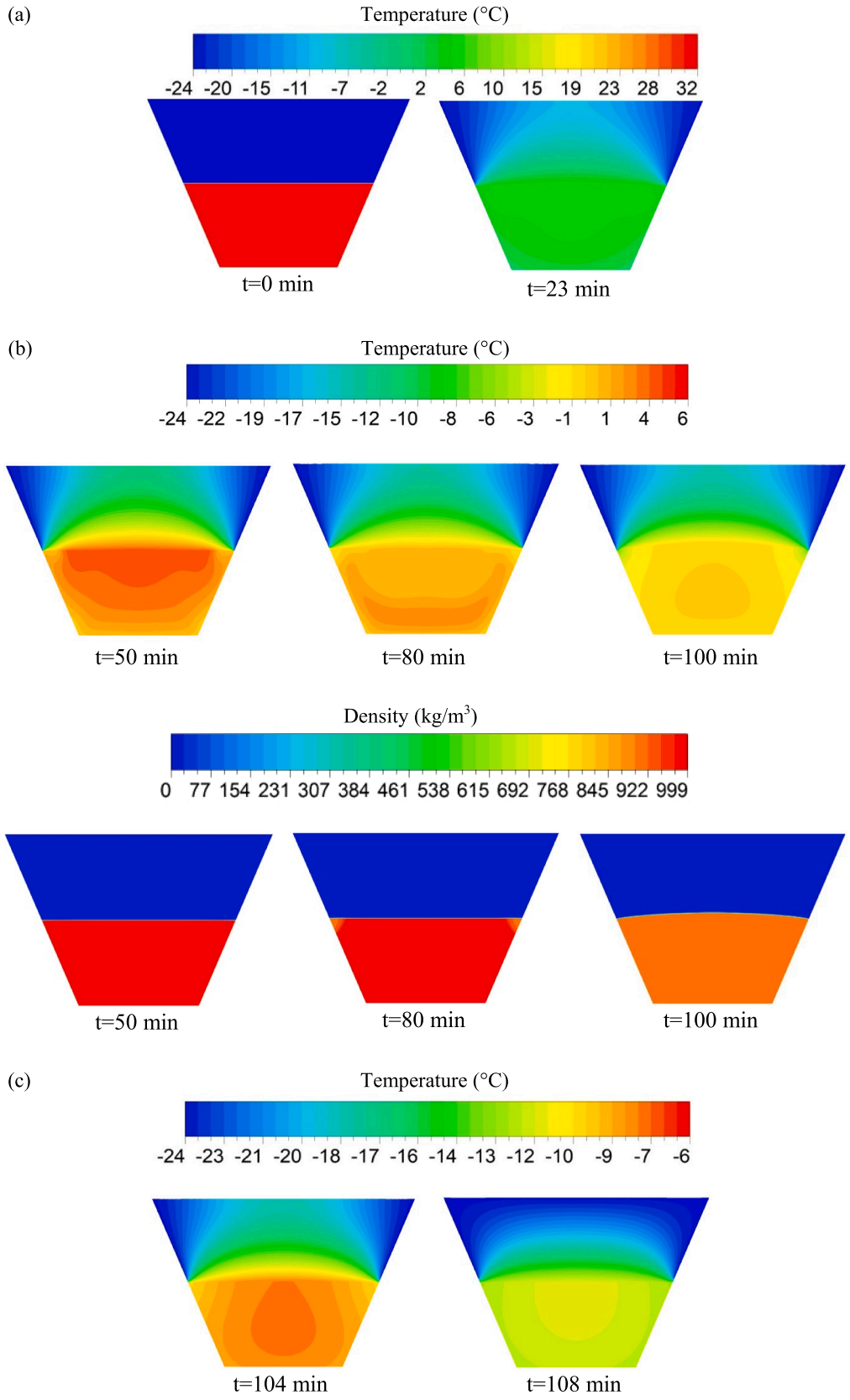

Fig. 15. Numerical results of the freezing process: (a) temperature contours at stage 1: water filling time (t = 0 min) and onset of water freezing (t = 23 min), (b) temperature and density contours at stage 2: water and ice mixture (t = 50 and t = 80 min), end of solidification (t = 100 min), and (c) temperature contours at stage 3: ice cube at −8°C (t = 104 min), ice cube at −12 °C (t = 108 min).

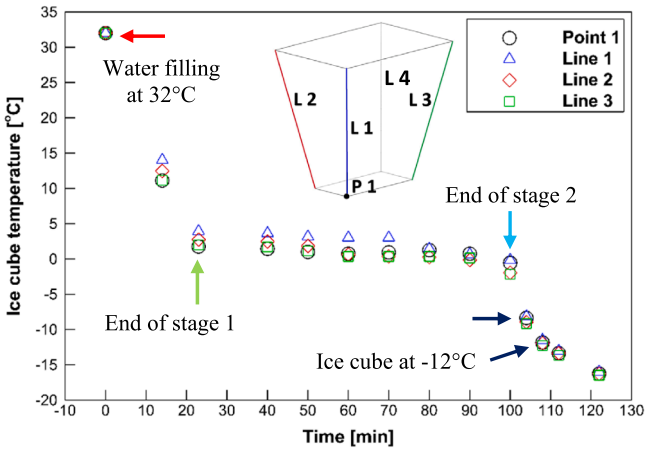

Fig. 16. Ice cube temperature at four positions considering water filling temperature of 32 °C and freezer temperature of −24 °C.

seen, water temperature rapidly decreases within 23 min until it reaches 0 °C at the edges of the water–air interface, in which the freezing process initiates. Fig. 15 demonstrates both the temperature and density distribution during stage 2. Solidification starts from the outer layers of the ice cube and after 80 min, the interface reaches the inner layers of water. At 100 min, all water is frozen and ice cube volume has increased due to solidification. The increased volume is shown by the induced curvature on the ice-air interface. According to Fig. 15, during stage 3, the ice cube rapidly reaches −8°C and −12 °C in 104 and 108 min, respectively. Under the same operating conditions, the ice tray reached −12 °C at ~ 100 and ~ 106 min according to experimental and theoretical data (see Fig. 12). his indicates a reasonable agreement between the theoretical, numerical, and experimental data.

Fig. 16 shows the temperature gradient inside the ice cube at four different positions during the freezing process—the temperature of point 1 in addition to the average temperature of lines 1–3. As seen in this figure, line 1 is located in the center of the ice cube, which has the highest temperature during the freezing process. In contrast, line 3 at the vicinity of the top and side surface of the ice cube receives the highest convective heat transfer coefficient—indicating the onset of freezing.

Fig. 17 shows the ice cube temperature as a function of ice cube height for lines 1–4. There is a temperature non-uniformity during the icemaking process. Ice has a higher thermal conductivity leading to a less steep temperature gradient compared to that of water. After reaching −8°C, the temperature inside the ice cube becomes uniform. It should be noted that water density increases by decreasing temperature until 4 °C and then lowers till it reaches 0 °C. Also, water experience a sudden decrease in density by solidification (i.e. density of water and ice at 0 °C are around 1000 and 920 kg/m^3 respectively). It is seen that before ice cube reaches the 4 °C, the top surface has the highest temperature in all lines. This is because colder water from top with high density is replaced with warmer water from bottom with lower density. Once the ice cube temperature drops below 4 °C, particularly after 80 min, the top surface temperature starts to decrease. This happens

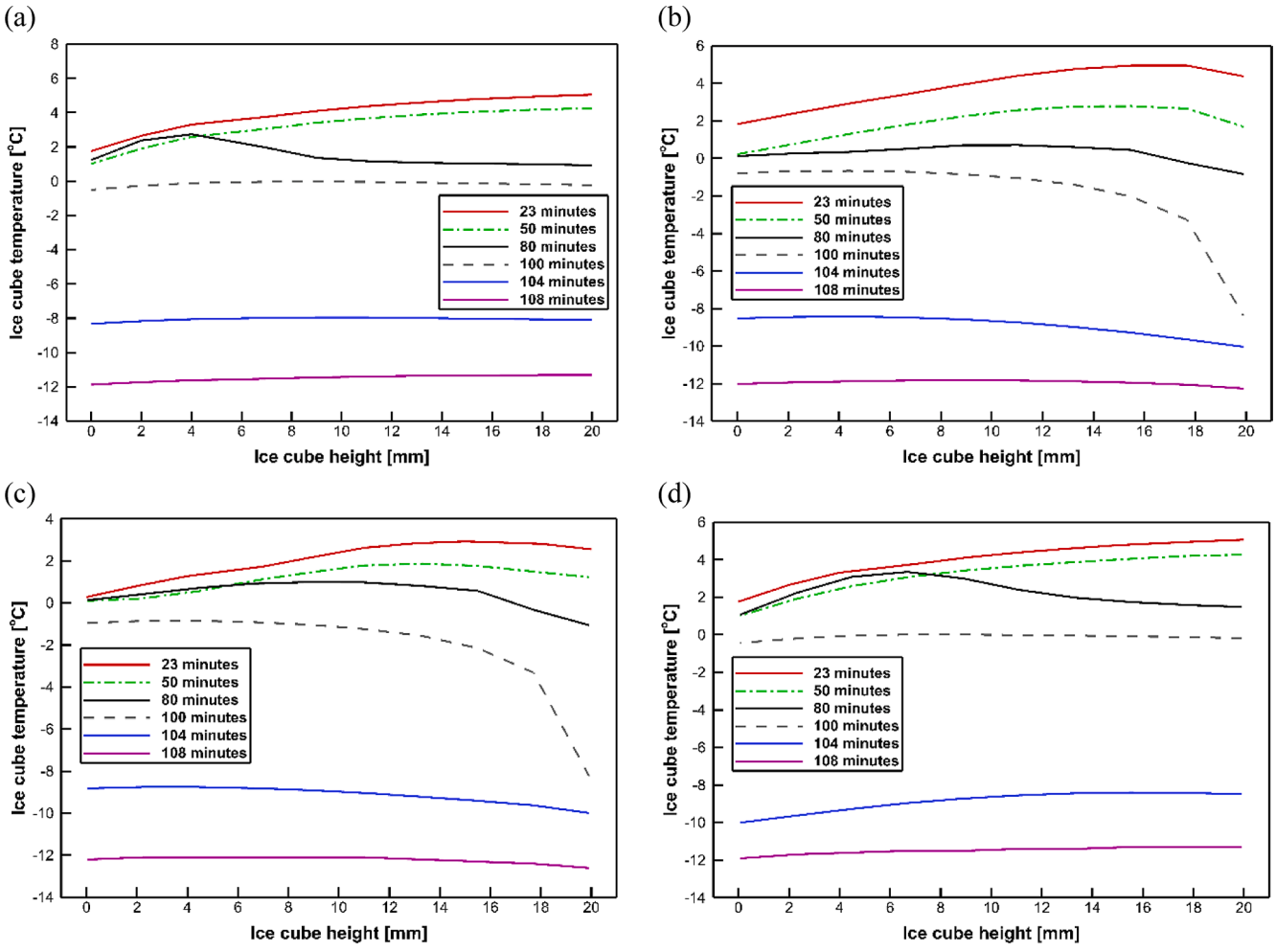

Fig. 17. Ice cube temperature as a function of ice cube height at various time intervals for four different positions of: (a) L1, (b) L2, (c) L3, and (d) L4.

because the colder water, with its lower density, tends to stay on the top surface of the ice cube. Temperature profile at 100 min better clarifies that freezing starts from the top side of the ice cube.

In order to eject the ice cubes from the ice tray to the ice bucket, a temperature for the ice tray should be defined. With the current icemaker, ice cube ejection occurs when the ice tray reaches the −12 °C. When the freezer air temperature is at −16 °C (see Fig. 14), temperature reduction of the ice tray from −8°C to −12 °C takes around 25 min. Thus, setting the ice removal temperature (based on the ice tray NTC sensor) at −8°C enhances the icemaking rate by around 18 %. It should be noticed that ice cubes are ejected at a temperature lower than 0 °C because although the outer layer of the ice cube is at 0 °C (i.e. where the icemaker sensor is located) the center of the ice cube still contains liquid water. Hence, ice cube should be ejected with surface temperatures under 0 °C. Furthermore, the icemaker temperature sensor is exposed to the freezing air around the icemaker and thus it is possible that the sensor records a temperature value which is lower than that of water in the ice cube. Furthermore, a safety factor should be considered to make sure that the ejected ice cubes are fully frozen. The results presented here indicate that an ice tray temperature set point of −8°C is sufficiently low to ensure that the water is fully frozen and the ice cubes can be ejected.

7. Conclusion

Embedding automatic icemakers in refrigerators ensures a steady ice supply and enhances energy efficiency. However, the literature lacks a comprehensive examination of the automatic icemaking process in domestic refrigerator-freezers despite these advantages. The present work investigated the icemaking process in a domestic freezer through theoretical, numerical, and experimental analyses. During the experimental stage, a practical approach is undertaken to assess how the icemaking process can be accelerated through more accurate setting of a temperature sensor responsible for ejecting ice cubes into the ice tray. The numerical simulation includes a three-dimensional transient model using the enthalpy-porosity and volume of fluid methods to map the solid–liquid front. It is found that the free convective heat transfer coefficient and, as a result, the icemaking process accelerate with decreasing freezer temperature. The solidification process starts from the vicinity of the top and side surface of the ice cube, which receives the highest convective heat transfer coefficient. The maximum temperature non-uniformity inside the ice cube with average temperature of −12 °C and −8°C is found to be 1.3 °C and 2 °C, respectively. The optimum ice removal temperature is found to be −8°C, which shortens the solidification process by 18 % and increases the total mass of ice made during a day by 20 %.

CRediT authorship contribution statement

Ali Akbar Ahmadi: Conceptualization, Methodology, Software, Validation, Formal analysis, Writing – original draft, Project administration. **Kamel Hooman:** Methodology, Investigation, Writing – original draft, Supervision. **Alireza Rahbari:** Conceptualization, Methodology, Formal analysis, Writing – review & editing, Supervision.

Declaration of competing interest

The authors declare that they have no known competing financial interests or personal relationships that could have appeared to influence the work reported in this paper.

Data availability

No data was used for the research described in the article.

References

[1] M.R. Lee, S.J. Kim, Quick ice-making control method of ice-maker for refrigerator ed, Google Patents (2006).
[2] F. Ghadiri, M. Rasti, The effect of selecting proper refrigeration cycle components on optimizing energy consumption of the household refrigerators, Appl. Therm. Eng. 67 (1–2) (2014) 335–340.
[3] M.M. Joybari, M.S. Hatamipour, A. Rahimi, F.G. Modarres, Exergy analysis and optimization of R600a as a replacement of R134a in a domestic refrigerator system, Int. J. Refrig 36 (4) (2013) 1233–1242.
[4] M. Tosun, B. Doğan, M.M. Öztürk, L.B. Erbay, Integration of a mini-channel condenser into a household refrigerator with regard to accurate capillary tube length and refrigerant amount, Int. J. Refrig 98 (2019) 428–435.
[5] B. E. D. Book, "Building Technologies Program, Energy Efficiency & Renewable Energy, US Department of Energy, March 2012," ed, 2011.
[6] T. Mahlia, H.H. Masjuki, R. Saidur, M. Amalina, Cost–benefit analysis of implementing minimum energy efficiency standards for household refrigerator-freezers in Malaysia, Energy Policy 32 (16) (2004) 1819–1824.
[7] J. Boeng, C. Melo, Mapping the energy consumption of household refrigerators by varying the refrigerant charge and the expansion restriction, Int. J. Refrig 41 (2014) 37–44.
[8] M. Mohanraj, Energy performance assessment of R430A as a possible alternative refrigerant to R134a in domestic refrigerators, Energy Sustain. Dev. 17 (5) (2013) 471–476.
[9] M. Rasti, S. Aghamiri, M.-S. Hatamipour, Energy efficiency enhancement of a domestic refrigerator using R436A and R600a as alternative refrigerants to R134a, Int. J. Therm. Sci. 74 (2013) 86–94.
[10] F.G. Modarres, M. Rasti, M.M. Joybari, M.R.F. Nasrabadi, O.J.M. Nematollahi, Experimental investigation of energy consumption and environmental impact of adaptive defrost in domestic refrigerators, Measurement 92 (2016) 391–399.
[11] V. Dmitriyev, V. Pisarenko, Determination of optimum refrigerant charge for domestic refrigerator units, Int. J. Refrig 7 (3) (1984) 178–180.
[12] K.M. Traeger, P.S. Hrnjak, Charge minimization of microchannel heat exchangers, University of Illinois at Urbana-Champaign, Air Conditioning and Refrigeration Center. College of Engineering, 2005.
[13] W.J. Yoon, H.W. Jung, H.J. Chung, Y. Kim, Performance optimization of a two-circuit cycle with parallel evaporators for a domestic refrigerator–freezer, Int. J. Refrig 34 (1) (2011) 216–224.
[14] M. Rasti, J.H. Jeong, A generalized continuous empirical correlation for the refrigerant mass flow rate through adiabatic straight and helically coiled capillary tubes, Appl. Therm. Eng. 143 (2018) 450–460.
[15] B. Palm, Refrigeration systems with minimum charge of refrigerant, Appl. Therm. Eng. 27 (10) (2007) 1693–1701.
[16] P. Hrnjak, A.D. Litch, Microchannel heat exchangers for charge minimization in air-cooled ammonia condensers and chillers, Int. J. Refrig 31 (4) (2008) 658–668.
[17] N. Agrawal, S. Patil, P. Nanda, Experimental Studies of a Domestic Refrigerator Using R290/R600a Zeotropic Blends, Energy Procedia 109 (2017) 425–430.
[18] C. Aprea, A. Greco, A. Maiorino, An experimental investigation on the substitution of HFC134a with HFO1234YF in a domestic refrigerator, Appl. Therm. Eng. 106 (2016) 959–967.
[19] J.M. Belman-Flores, A. Rodriguez-Munoz, C.G. Pérez-Reguera, A. Mota-Babiloni, Experimental study of R1234yf as a drop-in replacement for R134a in a domestic refrigerator, Int. J. Refrig 81 (2017) 1–11.
[20] A. K. Meier, "Energy use of icemaking in domestic refrigerators," 1996.
[21] I. Haider, H. Feng, R. Radermacher, Experimental results of a household automatic icemaker in a refrigerator/freezer, American Society of Heating, Refrigerating and Air-Conditioning Engineers, United States, 1996.
[22] D. A. Yashar and K.-J. Park, "Energy consumption of automatic ice makers installed in domestic refrigerators," NIST Technical Note 1697, National Institute of Standards and Technology, Gaithersburg, 2011 (https://is.gd/dGb25F, Accessed December 12, 2023).
[23] T. Michałek, T.A. Kowalewski, Simulations of the water freezing process–numerical benchmarks, Task Quarterly 7 (3) (2003) 389–408.
[24] A. Bourdillon, P. Verdin, C. Thompson, Numerical simulations of water freezing processes in cavities and cylindrical enclosures, Appl. Therm. Eng. 75 (2015) 839–855.
[25] F.R. Loyola, L.Z. Barboza, C.J. Hermes, Numerical simulation of water solidification in square ice trays: A simplified enthalpic formulation, in: Proceedings of the 25th IIR International Congress of Refrigeration, Montreal, Canada, 2019.
[26] G.M. Berno, F. Knabben, C. Hermes, Three-Dimensional Modeling of the Solidification Front in Ice Cubes. 19Th International Refrigeration and Air Conditioning Conference at Purdue, 2022.
[27] Y. Yao, K. Wu, R. Yang, H. Zhang, W. Yang, C. Li, Effects of surface temperature and Weber number on the dynamic and freezing behavior of impacting water droplets on a superhydrophobic ultra-cold surface, Appl. Therm. Eng. 236 (2024) 121705.
[28] S. Chang, H. Qi, S. Zhou, Y. Yang, Experimental and numerical study on freezing process of water droplets under surfaces with different wettability, Appl. Therm. Eng. 219 (2023) 119516.
[29] R.J. Moffat, Describing the uncertainties in experimental results, Exp. Therm Fluid Sci. 1 (1) (1988) 3–17.
[30] A.N.S.Y.S. Fluent, 17.1: Theory guide, ANSYS Incorporation (2016).

[31] X. Zhang, X. Liu, X. Wu, J. Min, Impacting-freezing dynamics of a supercooled water droplet on a cold surface: Rebound and adhesion, Int. J. Heat Mass Transf. 158 (2020) 119997.

[32] C. Popiel, J. Wojtkowiak, Simple formulas for thermophysical properties of liquid water for heat transfer calculations (from 0°C to 150°C), Heat Transfer Eng. 19 (3) (1998) 87–101.

[33] F.P. Incropera, A.S. Lavine, T.L. Bergman, D.P. DeWitt, Fundamentals of heat and mass transfer, Wiley, 2007.